Fluidic Fabric Muscle Sheets for Wearable and Soft Robotics

Mengjia Zhu,[1] Thanh Nho Do,[2] Elliot Hawkes,[3] and Yon Visell[1,3]

Abstract

Conformable robotic systems are attractive for applications in which they may actuate structures with large surface areas, provide forces through wearable garments, or enable autonomous robotic systems. We present a new family of soft actuators that we refer to as Fluidic Fabric Muscle Sheets (FFMS). They are composite fabric structures that integrate fluidic transmissions based on arrays of elastic tubes. These sheet-like actuators can strain, squeeze, bend, and conform to hard or soft objects of arbitrary shapes or sizes, including the human body. We show how to design and fabricate FFMS actuators via facile apparel engineering methods, including computerized sewing techniques that determine the stress and strain distributions that can be generated. We present a simple mathematical model that proves effective for predicting their performance. FFMS can operate at frequencies of 5 Hz or more, achieve engineering strains exceeding 100%, and exert forces >115 times their weight. They can be safely used in intimate contact with the human body even when delivering stresses exceeding 10^6 Pascals. We demonstrate their versatility for actuating a variety of bodies or structures, and in configurations that perform multiaxis actuation, including bending and shape change. As we also show, FFMS can be used to exert forces on body tissues for wearable and biomedical applications. We demonstrate several potential use cases, including a miniature steerable robot, a glove for grasp assistance, garments for applying compression to the extremities, and devices for actuating small body regions or tissues via localized skin stretch.

Keywords: artificial muscles, sheet-like actuators, fluidic actuation, wearables, fabric, textiles

Introduction

EMERGING SOFT ACTUATOR technologies are enabling applications in robotics, health care, haptics, assistive technologies, and many other areas. Such soft actuators can interface with, conform to, exert forces upon, or generate shape changes in complex or compliant structures.[1–3] Wearable soft robotic devices interfaced with the human body may prove valuable for rehabilitation, movement assistance, or virtual reality.[4–7] Soft actuators are also of interest for controlling motion in distributed and deformable structures. They can be used for tasks such as grasping, terrestrial locomotion, surgery, or underwater operation.[8–10] Such applications span systems of greatly varying size, ranging from millimeter-scale biomedical robots to large, deployable structures.[11,12]

Biological systems provide rich sources of information to guide the design of soft robots.[13] The motile capabilities of animals are enabled by composite systems of muscle, con-

nective, and other tissues. The forces and motions they can produce depend on the properties of individual muscle fibers, the arrangement of fibers, and the muscle morphology and attachments. Muscle morphologies vary widely. While fusiform shapes, such as the human biceps brachii, which can produce large-amplitude motion, are most common in robotics, many other morphologies exist. The present work is inspired by layered muscle sheets, such as the transverse abdominis (Fig. 1A), that compress or transfer forces around the torso.[14]

Here, we describe a new family of muscle-inspired actuators that we refer to as Fluidic Fabric Muscle Sheets (FFMS). They are composite fabric sheets that use an integrated fluidic transmission that comprised arrays of hollow elastic tubes to generate in-plane stresses or strains. We show how to design and fabricate these devices using apparel engineering methods. As we demonstrate, FFMS are stretchable, conformable, safe, efficient, and scalable. To situate this

[1]Media Arts and Technology Program, Department of Electrical and Computer Engineering, California NanoSystems Institute, and Center for Polymers and Organic Solids, University of California, Santa Barbara, Santa Barbara, California.
[2]Graduate School of Biomedical Engineering, Faculty of Engineering, University of New South Wales, Sydney, Australia.
[3]Department of Mechanical Engineering, University of California, Santa Barbara, Santa Barbara, California.
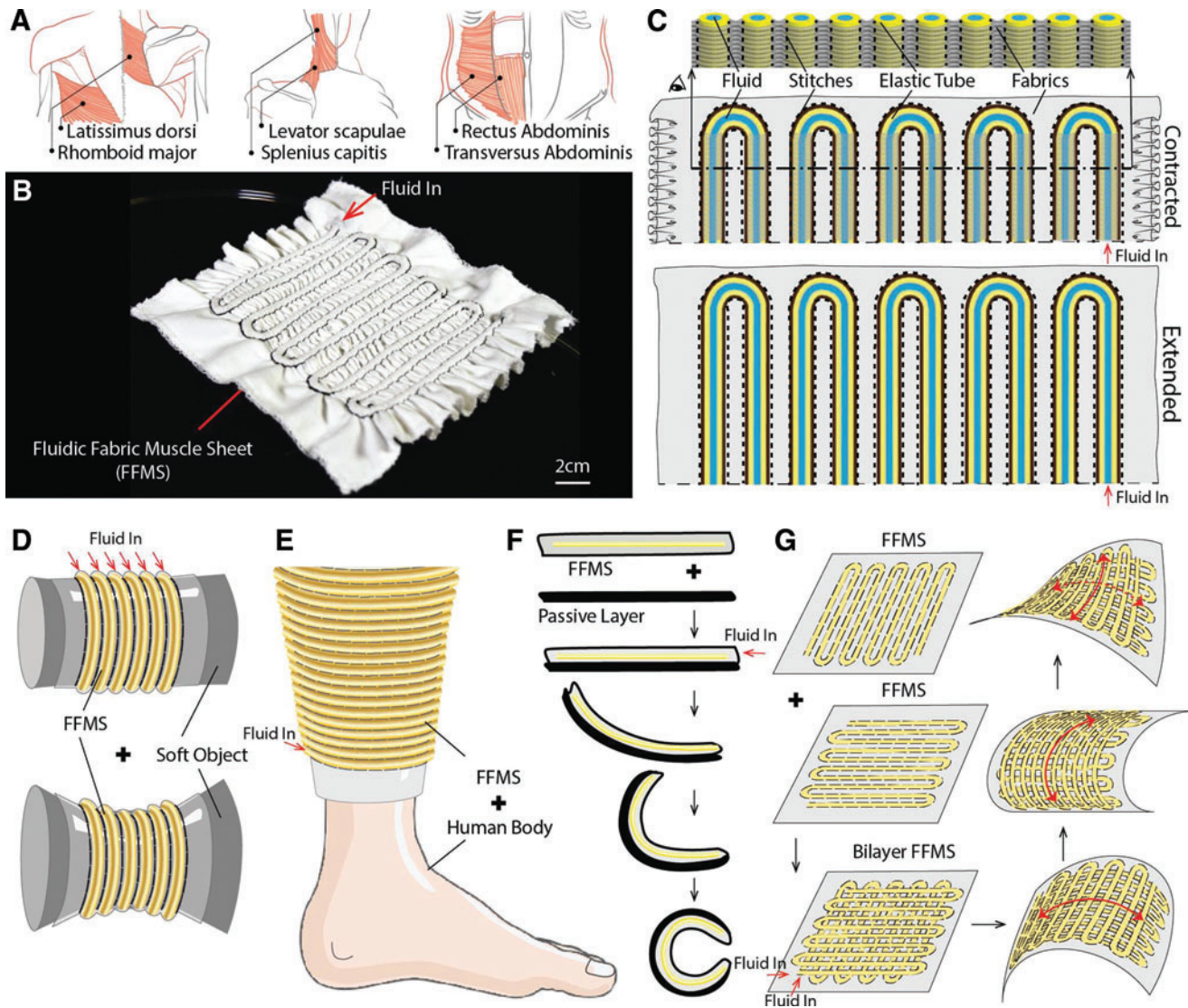
FIG. 1. **(A)** Examples of muscle sheets in the human body that inspired the design of FFMS.[61] **(B)** A functional prototype illustrating how FFMS are planar fabric structures analogous to muscle sheets. **(C)** FFMS comprise arrays of elastic tubes that function as fluidic transmissions. In this example, corresponding to the prototype of **(B)**, uniaxial extension is produced when fluid pressure is increased. **(D–G)** FFMS may be applied in a variety of ways (Fig. 10): **(D)** deforming a soft object, **(E)** compressing a limb, **(F)** bending a flexible structure, **(G)** in bilayer structures that generate morphological change, among many other possibilities. FFMS, Fluidic Fabric Muscle Sheets. Color images are available online.

work relative to prior research, we begin with a review of several related technologies.

Background

Many soft actuator technologies have been developed for applications in robotics, wearable devices, health care, and other areas. The FFMS actuators we present here build on prior research on soft fluidic actuators, including the sheet-like actuators described below. It is useful to compare the materials, operating principles, methods of design and fabrication, and performance characteristics of such devices.

Fluidic actuators. Fluidic actuation technologies have attracted considerable attention for use in soft robotic sys-

tems because of their intrinsic compliance and the ease with which the fluids that transmit stresses may be integrated into soft media.[15] Fluidic power may be delivered in the form of fluid pressure and volume changes via a variety of pumps or charged reservoirs, enabling such systems to be designed to match a wide range of requirements. Such devices can produce larger forces, displacements, or work densities than are feasible with many emerging functional materials technologies (Background section), facilitating practical applications.

Pneumatic artificial muscles, which generally shorten when filled with compressed air, come in many shapes and sizes.[16] An early, influential example is the McKibben actuator.[17–20] It comprises an airtight bladder with fiber constraints that cause it to contract when the internal volume is increased

through the application of pressure. The dimensions and working pressures of such actuators may be selected to match application performance requirements. However, maximum strains are typically <35%,[21,22] limiting applications.

Many soft, fluidic actuators have been designed for pneumatic operation via compressible gases. This causes energy to be stored in gas compression during operation, which can lead to undesirable, rapid energy release on failure. Gas compression also leads to thermodynamic losses. A smaller group of soft, fluidic actuators have used incompressible fluids. The FFMS actuators can use either approach. We review some of the advantages of hydraulic operation below.

Many other variations on the idea of combining fluidic actuation with fiber constraints have been investigated.[23,24] Recently, it has been observed that much larger strains can be realized—approaching 300%—by means of actuators that contract when the internal volume and pressure are reduced, in a manner inverse to the McKibben design. Such devices, including the Inverse Pneumatic Artificial Muscle (IPAM)[25] and Hydro-Muscle Actuators,[26] integrate anisotropic components that cause them to lengthen when pressurized.

We leverage just such an ''inverse'' fluidic actuation strategy in the FFMS actuators described here. In contrast to the typically uniaxial and tubular forms of prior devices, which evoke fusiform muscle structures, FFMS actuators are actuated fabric-based structures, similar to muscle sheets. Anisotropic constraints in FFMS actuators are provided by the fabric structure. Different fabric patterns and assemblies can be used to realize a variety of actuation modes, including uniaxial actuation, bending, multiaxis actuation, shape changing, and compression.

Several methods for creating mechanical anisotropies with fabrics have been previously investigated to improve the performance of fluidic actuators in devices based on individual tubes,[26] air bladders,[27] or other structures. In most cases, this is achieved through the intrinsic anisotropy of integral fibers. Fiber reinforcement of the elastomer can be designed to produce desired anisotropy, and hence motion, by specifying the threading angle of the fibers,[23,24] although this complicates fabrication.

Other soft, fluidic actuator designs, including origami-inspired devices, grow longer when positive pressure is applied.[28] However, the maximum forces that can be reproduced are limited by buckling instabilities.[29] Vacuum-driven soft actuators have also been realized, attaining large peak stresses,[30] but often involve large changes in the cross-section area.

Other transduction principles for soft actuators.

Many other methods of soft actuation have been investigated, each involving different trade-offs in performance. Shape memory alloys yield strains of up to about 5% when heated.[31] They can also yield larger strains in other configurations, such as coils.[32] Other thermally actuated transducers have been based on shape memory polymers, nylon, polyethylene, or other fibers.[33–35] Such actuators often yield low efficiencies or low-actuation speeds due to the thermal processes underlying actuation.

Other devices based on shape memory polymers[36,37] or electroactive polymer technologies, including ionic polymer/metal composites,[38–40] have been designed to yield high strains, but typically only generate small forces. Soft, electrostatic actuators, including dielectric elastomer actuators, are fast and can be designed to produce large strains[41] but require high voltages and carefully controlled fabrication processes and mechanisms that preclude their use in some applications. Variations on such actuators that use fluidic electrodes overcome some of the fabrication and design challenges involved in using such actuators, but high voltages are nonetheless required.[42] Electromagnetic soft actuators can operate at low voltages,[43,44] but often yield low work rates or require an external magnetic power source.[45,46]

Another approach to producing high forces and strains in soft, actuated structures is based on tendon- or Bowden-cable transmissions.[47–49] Achieving high-performance actuation and control with such devices depends on cable routing and friction management. In addition, careful design is needed to ensure that the stresses produced are appropriately distributed.

Sheet-like soft actuators.

Various sheet-like soft actuators have been developed using actuation methods paralleling those described above. Several groups have produced such sheet-like actuators based on shape memory alloys or thermally actuated nylons, but the trade-offs between actuation time, forces, and strains limit the feasible mechanical power and speed, and reduce efficiencies.[50–53] In addition, the temperatures or heat exchange requirements may limit wearable applications.

Multilayered artificial muscles made of electrostatic sheet actuators have been designed to produce large forces at moderately high voltages, but require careful control over their motion during actuation, precluding out-of-plane deformation.[54] Dielectric elastomer actuation principles have also been used to realize compact sheet-like soft actuators, although large voltages (>1 kV) are normally required.[55,56]

Sheet-like, fluidic soft actuators have been designed by assembling discrete pneumatic artificial muscles within a fabric, pouch, or other assembly.[57] One configuration integrated McKibben muscles within fabric layers.[2] Another consisted of thin McKibben muscles that were woven into fabric structures.[58] When driven to produce contraction along the axis of each muscle, the actuators expand, causing undesired increases in thickness, adversely affecting potential conformable or wearable applications and reducing efficiency. Other designs have resulted in low forces that preclude many applications.[59] In contrast, the FFMS actuators presented here increase in nominal length, or decrease in contraction force, when fluid pressure is applied. This is achieved with negligible tangential expansion over the normal operating range of the actuator.

Other authors have used parallel cables or strings routed within fabric structures to create sheet-like actuators.[60] Such designs can produce thin, fabric-like actuators, but require careful attention to cable actuation and friction management to ensure that dynamic, fast, and reversible actuation is possible. Because FFMS actuators transmit stresses via integral fluids, losses, due to viscosity and channel length (Analytical Modeling section) remain within ranges that permit highly dynamic operation.

Contributions

This article presents FFMS, a new soft actuation technology. FFMS are planar, multimodal soft actuators that are analogous to muscle sheets. Their design also builds upon prior ''inverse-type'' uniaxial actuators with tubular shapes

that can be compared with fusiform muscles. Here, we describe the design and fabrication of FFMS and show that this planar paradigm opens many new actuation capabilities and applications. These low-cost devices admit multiple design options at multiple scales, facile fabrication, can conform to curved structures, produce large work densities, and achieve fast response times.

Design, fabrication, and modeling. We show how to design composite fabric structures to realize mechanical anisotropies that enable FFMS to generate patterns of local contractions in a conformable, planar surface as fluid is withdrawn. FFMS can be efficiently fabricated using apparel engineering methods, including pattern making, computerized sewing, and wrinkling, and through the integration of a fluidic transmission based on hollow elastic tubes (Figs. 2–4). We describe several alternatives for their design and assembly. We analyze the effects of fabric selection and wrinkling, tube routing, thread selection, and stitching selection, all of which can be used to tailor functionality and performance. We also present a simple mathematical model that proves effective for predicting their performance and aiding design.

Actuation capabilities. FFMS actuators may be scaled to different sizes, depending on design requirements. We demonstrate actuators with dimensions ranging from 1 to 34 mm in thickness, and 30 to 1000 mm in length, yielding forces that can exceed 150 N, and that can produce forces

more than 115 times greater than their weight. FFMS actuators can also produce uniaxial engineering strains exceeding 100%. Laboratory prototypes perform consistently in durability testing during 5000 cycles or more, with <5% change in displacement (Figs. 5–8).

Applications. We demonstrate their use in actuating various bodies and mechanisms, and in configurations that perform multiaxis actuation, including in- or out-of-plane bending and shape change (Fig. 9). We also demonstrate applications of FFMS methods for realizing low-profile, fabric-based actuators for new devices that exert forces on body tissues for wearable and biomedical applications. These include a glove for grasp assistance, devices for compressing small body regions or tissues, and devices for providing haptic compression or skin stretch to a finger, arm, or leg.

Compression garments formed from these actuators can produce dynamic compressive pressures that scale to high, predictable values; we demonstrate prototypes that easily generate compression of 4 kPa, which is sufficient for haptic feedback, meeting requirements needed for many musculoskeletal, circulatory, wound, and lymphatic compression therapies, including peristaltic compression modes (Fig. 10).

Design Concept and Operating Principle

FFMS actuators generate stresses or strains in a composite fabric sheet when charged with a pressurized fluid. The fluid may be compressible (pneumatic operation) or incompressible
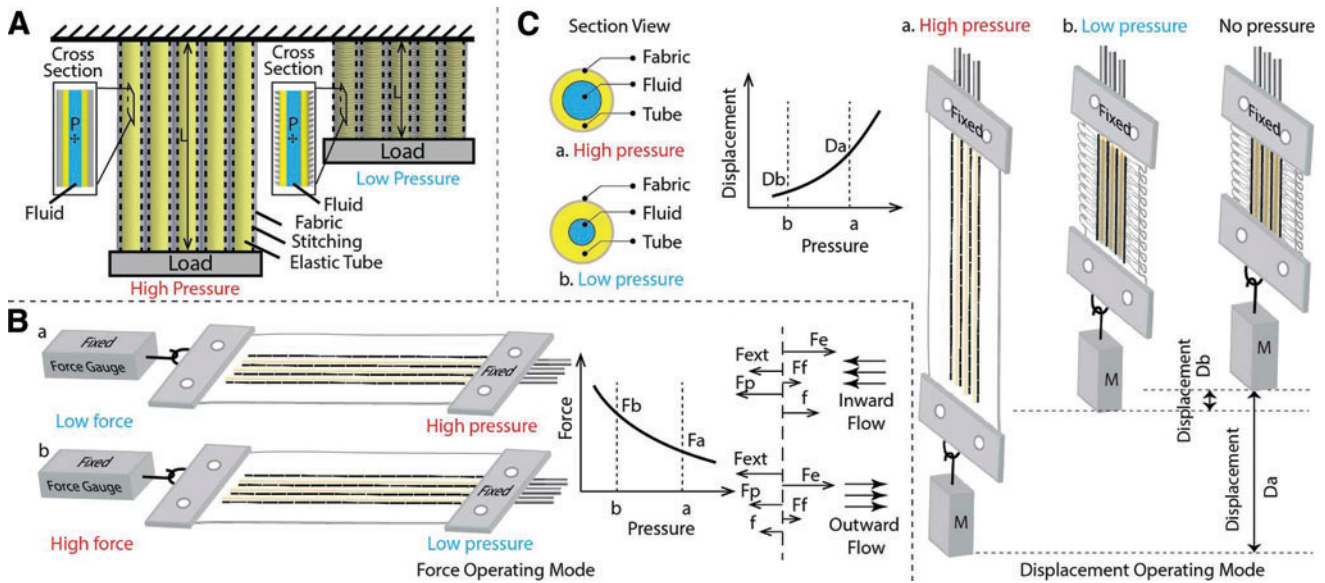

FIG. 2. FFMS: concept and operating principle. **(A)** Hollow elastic tubes are integrated in a composite fabric structure. The tubes are routed in fabric conduits that provide circumferential constraints, due to stitching. *Left:* when pressurized fluid is pumped into the elastic tubes, the tubes cannot swell radially due to the constraining stitches and thus can produce a lengthening, similar to a relaxing sheet of muscle. *Right:* when the fluid pressure is removed, stored elastic energy in the hollow tubes and elastic fabric is released, and the entire textile shortens, like a contracting sheet of muscle. *P* and *L* represent fluid pressure and actuator length, respectively. **(B)** *Left:* when the FFMS are operated to work against a load, as in the isometric configuration shown here, forces are produced. *Middle:* high pressures produce low forces, and vice versa. F_b and F_a correspond to states *a* and *b* in **(B)**. *Right:* a simple illustration of the generation of axial forces. We present a mathematical model in a subsequent section. **(C)** *Left:* cross-section view of a single channel in the displacement operating mode. Wall thinning may result as the elastomer length increases. *Middle:* in displacement mode, higher pressures produce larger displacements, and vice versa. *Right:* in such a displacement mode, the FFMS may be used to do external work, such as lifting a mass, as shown here. Color images are available online.
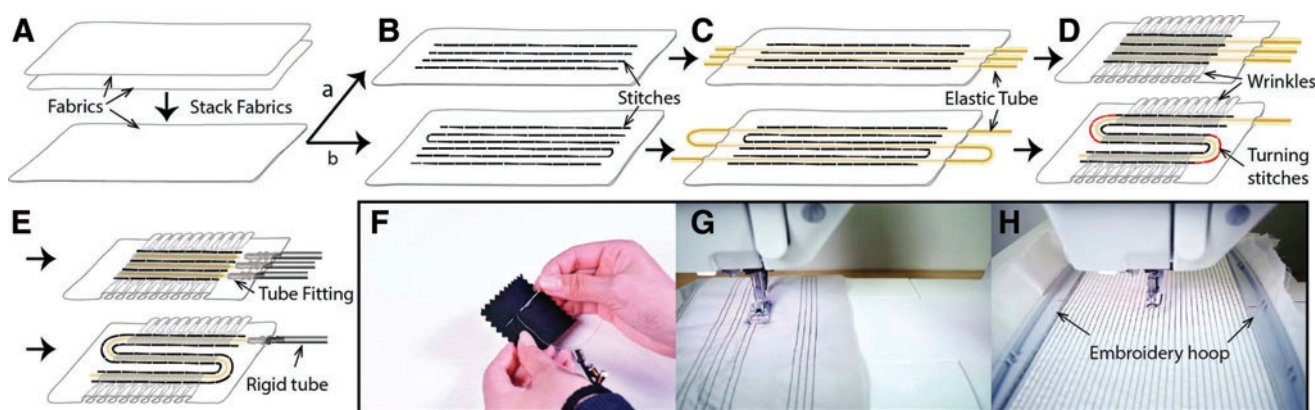
FIG. 3. Fabricating planar fluidic fabric muscles involves several steps based, in part, on apparel engineering methods. For configurations based on nonstretchable fabrics, the fabric layers are first aligned and stacked. **(A)** The routing of elastic tubes is designed, and layers are stitched to form conduits **(B)** in a pattern that determines the routing. The stitched patterns can realize single **(B.b)** or multiple **(B.a)** tube routings. The elastic tubes are then threaded **(C)** through the resulting fabric conduits. **(D)** For nonstretchable fabric layers, the fabric structure is wrinkled. **(E)** A port is established at one end of each channel, whose remote end is then sealed. The stitching may be done via **(F)** hand sewing, **(G)** machine sewing, or **(H)** computerized embroidery. Color images are available online.
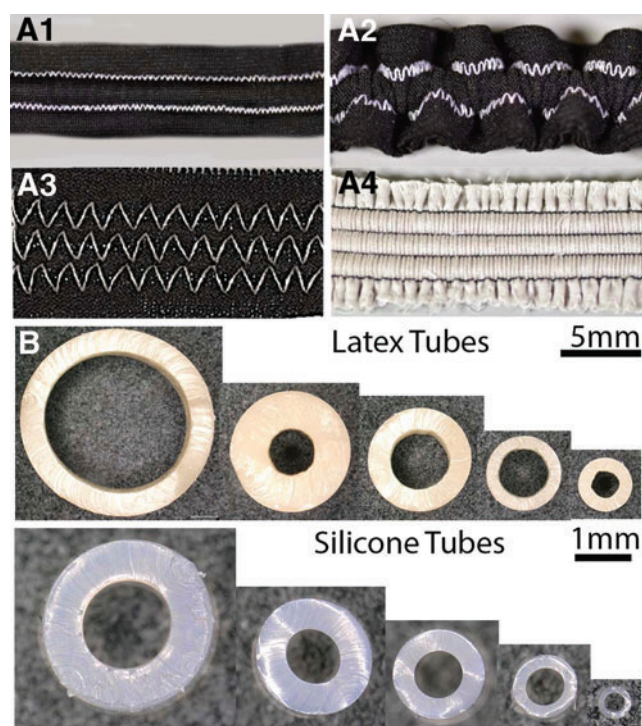

FIG. 4. **(A1–A4)** Four representative FFMS prototypes illustrating different fabric and stitch combinations. **(A1)** Two-way stretch fabric using zig-zag side-stitches without wrinkling. **(A2)** Two-way stretch fabric using zig-zag side-stitches with wrinkling. **(A3)** Two-way stretch fabric using zig-zag cross-stitches without wrinkling. **(A4)** Nonstretch fabric using straight side-stitches with wrinkling. **(B)** Cross-section images of several commercially available tubes made of latex (*top*) and silicone (*bottom*, note the smaller scale). The *outer* diameter of the silicone tube can reach submillimeter scales. Color images are available online.

(hydraulic operation); we compare the relative merits of each later in the article.

The routing of stresses and strains is accomplished via an integral fluidic transmission composed of hollow elastic tubes. The fabric assembly directs stresses along axis of channels that are sewn into the fabrics. As fluid is pumped into the elastic tubes, their internal volume is forced to increase. Circumferential constraints imposed by the fabric cause the increased fluid volume to produce a nominal lengthening of the structure along the axis of each tube (Fig. 2A). This causes elastic energy to be stored in the tube fabric structure. As the fluid pressure or volume is reduced, the stored elastic energy is released. When the FFMS are working against a load, this reduction in pressure yields a contraction force. Thus, while increased pressure produces a lengthening of the FFMS, external forces are normally produced via contraction, similar to biological muscles (Fig. 1A).[61]

As we demonstrate, the same principle can be used to realize FFMS actuators that operate in a hydrostatic mode, similar to muscular hydrostats such as the tongue of many animals or trunk of the elephant. The ranges of forces and displacements that can be produced depend on the dimensions of the FFMS, operating range of applied fluids, actuation mode, and materials involved. We present a simple mathematical description of the effects of these factors below.

Depending on actuation requirements, FFMS can be operated to produce forces or displacements. In force mode (Fig. 2B), a muscle is prestretched against a load via constraints at both ends. High fluid pressures produce low forces, and vice versa. Stresses act along the longitudinal axis of the elastic tubes. This can yield axial forces, or compression forces, when the FFMS are wrapped in a nose-to-tail configuration around an object, such as a human limb (Fig. 10F).

FFMS may also be used to generate large strains or displacements (Fig. 2C). Changes in displacement can be used to displace loads or to alter the shape of a structure through differential stresses or strains. Due to the radial constraint imposed by the composite fabric structure, a change in fluid volume creates a change in length. The relationship between the fluid volume in the FFMS and the channel length is approximately
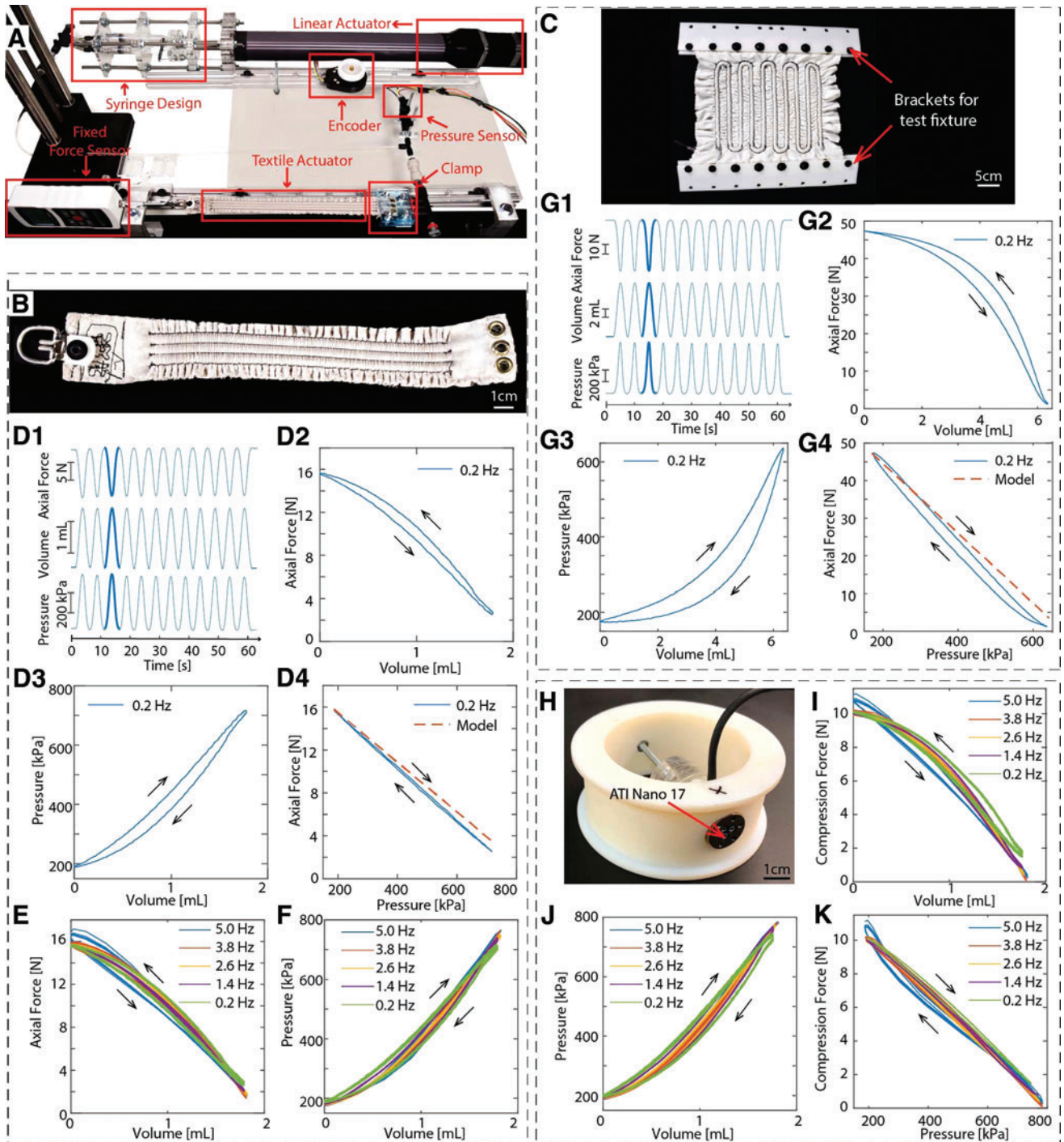
FIG. 5. Force testing. **(A)** Apparatus for axial force testing. **(B)** Three-channel FFMS. **(C)** Ten-channel FFMS with brackets for test fixture. **(D–F)** Results for the three-channel FFMS demonstrated consistent performance over repeated actuation, similar behavior at different actuation speeds, and surprisingly good agreement with the analytical model. **(G1–G4)** The larger, 10-channel FFMS yielded similar results to those that we obtained with the 3-channel device. The force range was 0–50 N. The longer fluid circuit yielded slightly greater response latency. **(H)** Compression force testing apparatus. **(I–K)** The device produced compressive forces of 0–10 N, as 0–2 mL of fluid was withdrawn. The results were consistent with our analytical model and varied little with actuation speed. Color images are available online.

linear (see the Results section). Such a displacement can be used to perform mechanical work. As we show, in multilayer structures, it can also be used to effect changes in the intrinsic shape of an FFMS assembly. Together, these unique capabilities make FFMS amenable to various applications.

Fabrication

The fabrication of FFMS actuators involves three main steps. Construction, patterning, and assembly of a multilayer textile structure, routing of elastic tubes in the patterned fabric structure, and sealing and attachment of tube fittings,
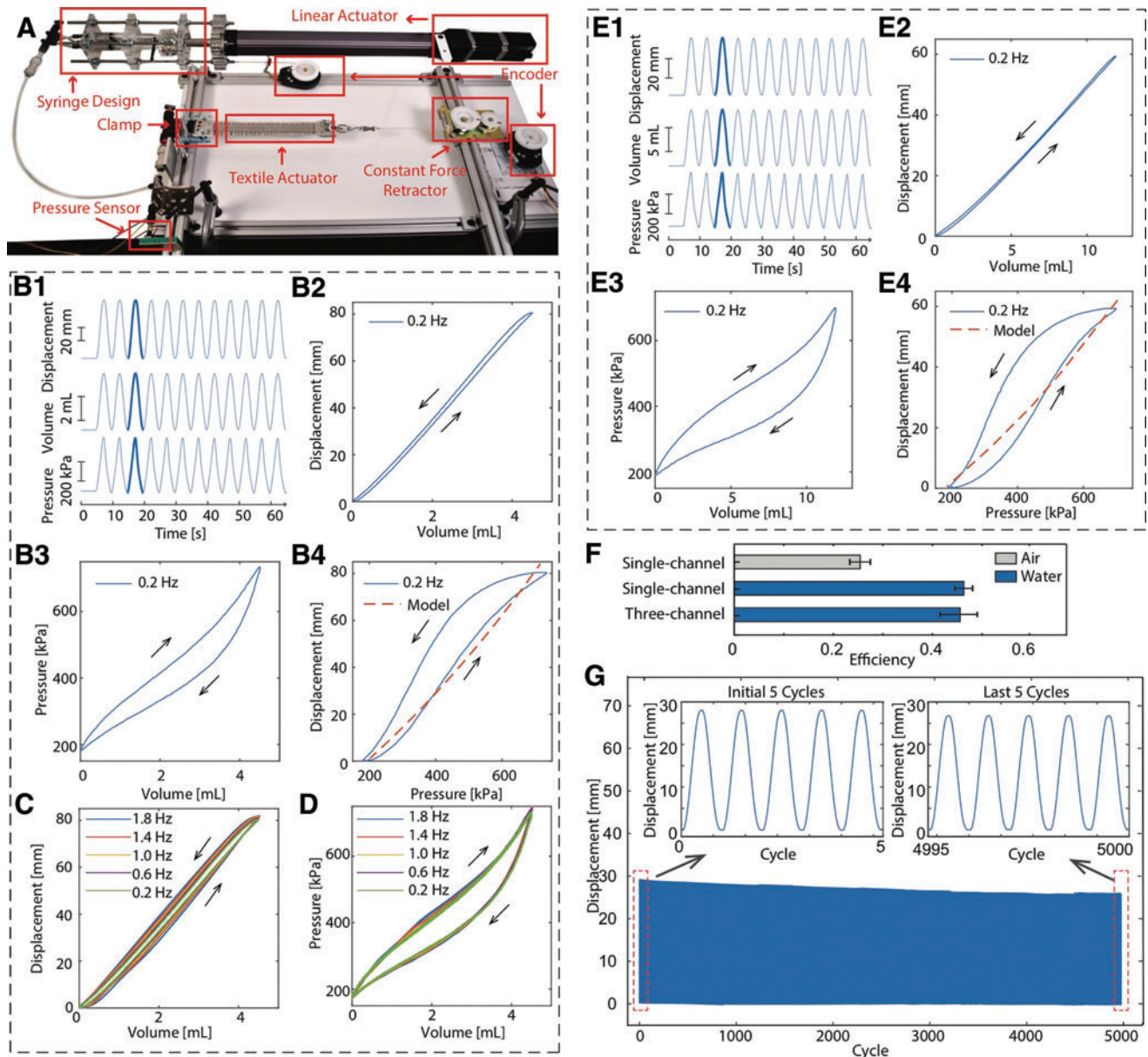
FIG. 6. Displacement and compression testing. **(A)** Apparatus for displacement testing. **(B–D)** Results for the three-channel FFMS were consistent over repeated actuation. Similar behavior was observed for different actuation speeds. The pressure/displacement relationships were consistent with analytical predictions, despite dynamic effects, including hysteresis (Analytical Modeling section). **(E1–E4)** Results for the larger, 10-channel FFMS were similar to those for the smaller FFMS. **(F)** Hydraulic operation with water was more efficient than with air. Similar efficiencies were measured for actuators with one and three channels. Error bars: 95% confidence intervals. **(G)** Durability testing revealed consistent performance over 5000 actuation cycles. A 5% reduction in displacement was observed after this period, which we attributed to initial actuator relaxation. Color images are available online.

as illustrated in Figure 3A–E. The figure highlights a process based on a configuration of nonstretchable fabrics with stitching parallel to the channels. Other stitching patterns suitable for stretchable fabrics are discussed in the Material Selection section below.

In the first step, the fabric layers are aligned and stacked. The layers are then stitched to form conduits between the fabric layers to allow tube insertion. The stitching patterns can be designed to realize configurations via a single tube and single fluid input port (Fig. 3B.a), or multiple tubes, enabling separate, independently addressable channels (Fig. 3B.b). The

routing of channels in the fabric determines the distribution of strain and stress within the composite textile, which need not be uniform. To radially constrain each tube, the conduit should possess a width equal to half of the tube diameter.

Different sewing methods can be used: hand sewing (Fig. 3F), machine sewing (Fig. 3G), and computerized embroidery (Fig. 3H). When the pattern size fits within machine limits, computerized embroidery is preferred. It provides great accuracy, flexibility, and efficiency. When embroidery is impossible, machine sewing may be used. This involves manual movement of the fabric under the sewing foot. This is
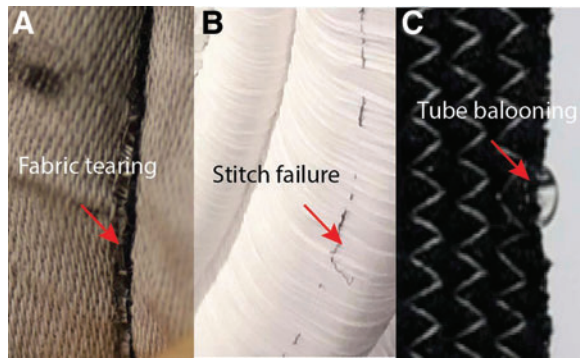
FIG. 7. Examples illustrating failure modes. **(A)** Fabric tearing at stitch locations. **(B)** Stitching failure between fabric conduits. **(C)** Tube ballooning between stitch locations. Color images are available online.

often the best option when stitching long actuators or very large surface areas. Hand sewing is the least efficient method, but can accommodate complex paths or nonflat fabric surfaces, as are involved when stitching the turning stitches that we apply following tube insertion (Fig. 3D).

After sewing, the tubes are threaded through the conduits via a slender rod inserted into an end of the elastic tube. The fabric is then wrinkled along the length of the tubes to accommodate stretching. We have found that this wrinkling can readily be performed in a uniform, controlled manner. Together, the proportion of wrinkling and elastic properties of

the fabric and tube determine the maximum length of the muscle. This process is best suited to nonstretchable fabrics. If stretchable fabrics are used, the wrinkling step may be omitted.

In a next step, one end of the elastic tube is sealed with a fixture, such as a knot, while the other is connected to a barbed tube fitting that allows the fluid to be supplied to the muscle. For large-scale FFMS (Fig. 8A, B), one end of the tube may be sealed with a solid barbed end plug, rather than a knot, while the other end is connected to a barbed tube fitting. To strengthen the connection between the fitting and the elastic tube, clamps may be applied. In the next step, air is purged from the channels. To stabilize the mechanical response, the muscle is fully extended and contracted several times before the first usage.

Material Selection

The performance of FFMS actuators depends on the selection of elastic material, fabric material, and stitching pattern. The working ranges of displacements and forces are determined by the applied fluid pressure range, the fabric and elastic tube material properties and sizes, and the manner of patterning and assembly.

Fabric and stitch selection

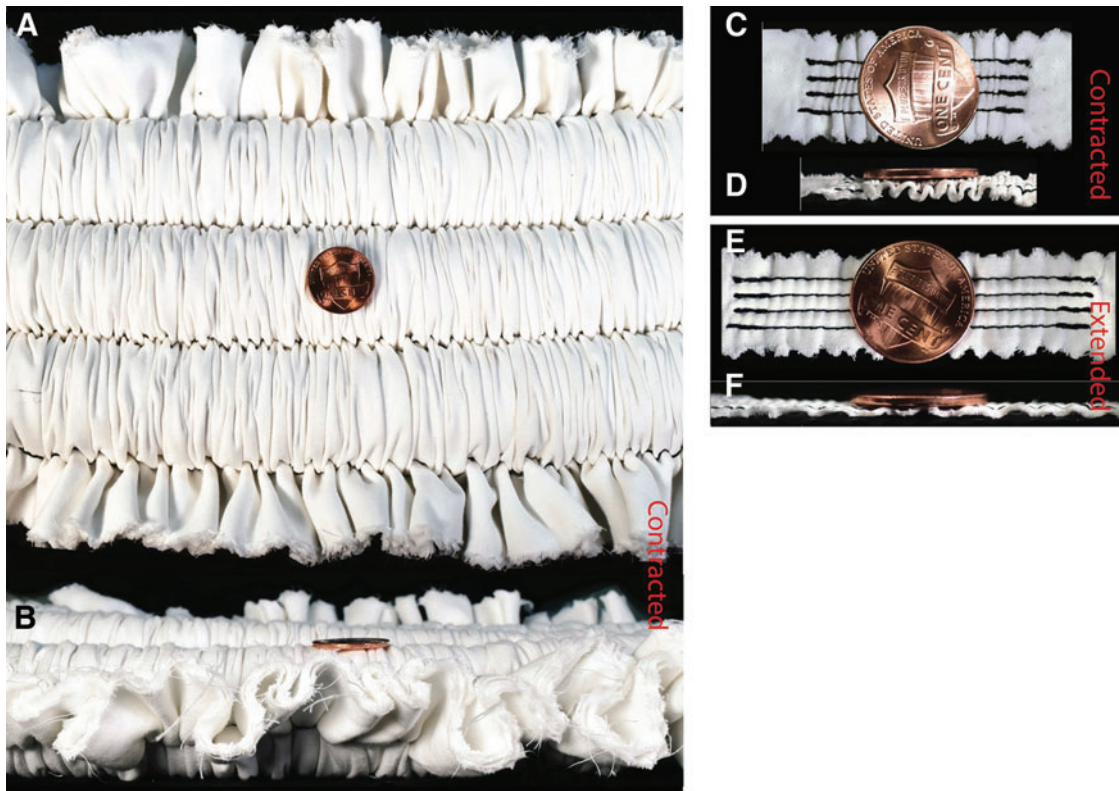Forces and motions produced by the FFMS are determined by the relative magnitude of stored energy generated by the

FIG. 8. FFMS actuators are readily scaled to small and large sizes. **(A, B)** A large example, consisting of 34.0-mm-thickness FFMS (**A:** top view, **B:** side view), shown in contracted state, was sufficient to lift 15 kg (Fig. 10). **(C–F)** A small example in contracted (**C, D**) and extended (**E, F**) states; the thickness when extended is 1.0 mm. The large and small actuators were fabricated using the same general process. A penny is used to illustrate the relative scale. Color images are available online.
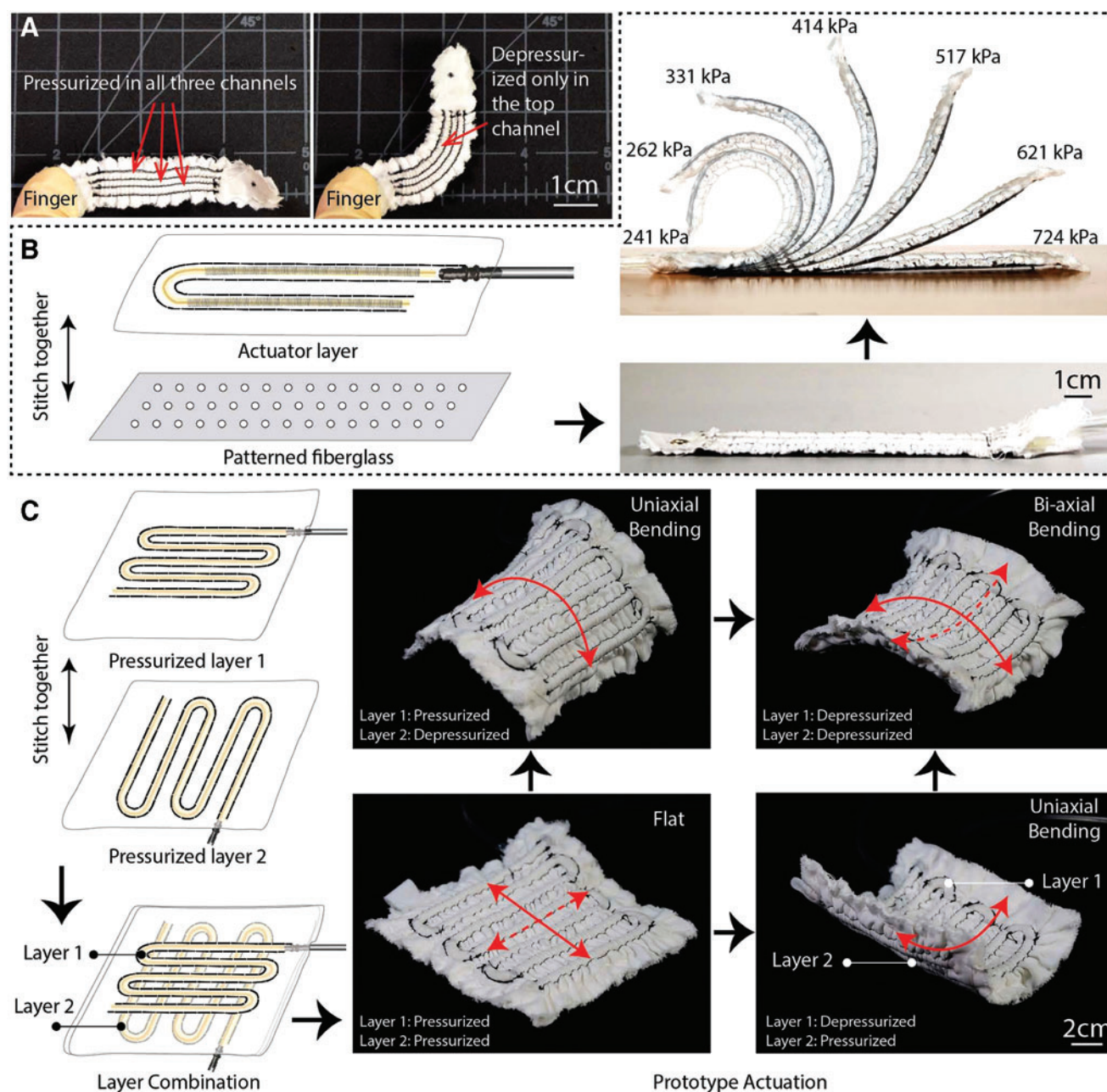
FIG. 9. Composite or multiactuated FFMS can realize dynamic, multimodal bending motion or shape change. **(A)** In-plane rotation realized by differential pressurization of multiple fluid channels. **(B)** Out-of-plane bending is realized by combining FFMS with a second, passive layer with specified bending stiffness. **(C)** Biaxial bending is realized via a composite of two, orthogonally oriented FFMS actuators. Color images are available online.

elastic tubes and the fluid pressure. To achieve the desired dynamic range of forces and motions, the axial stretchability of the fabric conduit should be maximized, while the radial expansion of the elastic tube in the operating range of fluid pressures should be minimized. A firm circumferential constraint is needed to ensure that stresses due to the fluid are directed along the axis of the tube and do not result in the tube expansion.

Based on these criteria, an ideal fabric structure should possess negligible stiffness in the axial direction of the tube. This can be achieved through the use of nonstretchable fabrics, such as cotton weaves, in tandem with the wrinkling process described above. Stretchable fabrics may be used together with across-tube stitching, which can provide a radial constraint. Stretchable fabrics are uniaxially elastic (two-way stretch) or biaxially elastic (four-way stretch). These fabrics are often made of elastic fibers, such as Spandex, that are spun into stretchable yarn, and integrated along weft, warp, or both directions of the weave, yielding one- or two-way stretch fabric, respectively.

Alternatively, either elastic or nonelastic fibers may be used to create a knit. In a knit, stretchability depends on the design of the looping structure. This typically results in bi-axial stretchability. The axial stretchability of FFMS fabric

FIG. 10. Demonstrations. **(A, D, E)** Miniature soft actuators for linear motion control or compression, capable of **(A)** lifting a small mass, **(D)** compressing small tissue areas, or **(E)** providing tactile feedback via skin stretch. *Inset*: skin stretch was easily perceived. **(B)** FFMS actuators can perform large mechanical work. A 10-channel device lifts a 3 kg mass. A three-channel structure (inner tube radius 2 cm) lifts a 15 kg cinder block and chain at pressures <276 kPa. **(C)** FFMS actuators can be integrated with fiberglass sheets to provide assistance for finger bending motion. **(F, G)** FFMS can be used for compression garments for health care, training, and haptics. **(F)** A compression band yields uniform pressure on the upper limb, easily matching pressures provided by blood pressure cuffs. **(G)** A compression garment for the lower limb comprises three independently addressable sections (*dashed boxes*). Pressure variations can yield peristaltic motions suitable for undulatory massage in therapies for lymphatic and blood circulation,[76] such as lymphedema[77] or venous closure.[78] Color images are available online.

structures using stretchable fabrics can also be improved through the application of wrinkling, if required.

The routing of stresses or strains within the FFMS is achieved via fabric conduits formed from stitching applied to the fabric sheets. The stitching involves three main factors: thread material, stitch type, and stitch pattern. Near the elastic tubes, the stitching permits the fabric to impose a circumferential constraint. This ensures that fluidic stress or strain is

directed along the axis of the tube (see the Design Concept and Operating Principle section).

Two design criteria are involved. First, the stitching must be strong enough to constrain the fabric conduit around the elastic tubes over the entire operating regimen of the FFMS. Second, it must accommodate large strains along the axial direction of the tube. Different stitch designs and fabric choices can be used. Their selection depends on application
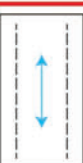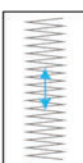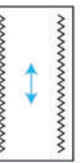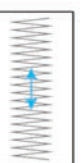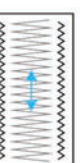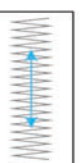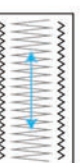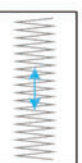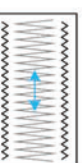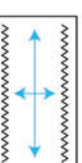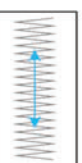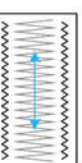
Stitches / Fabrics	No Fabric Wrinkling			With Fabric Wrinkling			Advantages	Disadvantages
	Side Stitch	Cross Stitch	Side + Cross	Side Stitch	Cross Stitch	Side + Cross		
Non-stretch				(red box)			No radial expansion.	Wrinkling required for stretchability.
Two-way stretch							Wrinkling not required for stretchability.	Difficult to align layers of fabrics accurately.
Four-way stretch							Wrinkling not required for stretchability.	Must use cross stitch to prevent radial expansion.
Advantages	Easy to insert tube.	Better constraint in radial direction.	Best constraint in radial direction and between stitches.	Easy to insert tube. Large wrinkling possible (allowing large elongation).	Better constraint in radial direction.	Best constraint in radial direction and in between stitches.		
Disadvantages	Slight radial expansion exists, expecially for knit fabrics.	Difficult to insert tube. Tube may balloon between stitches.	Difficult to insert tube.	Permits radial expansion, expecially for knit fabrics.	Difficult to insert tube. Limited wrinkling.	Difficult to insert tube. Limited wrinkling.		

FIG 11. Stitch and fabric selection for FFMS actuators. *Red arrows* represent the stretch directions of the fabrics, and *blue arrows* represent the stretchability of the assembled FFMS. *Longer arrows* denote greater stretchability. The configuration in the *red box* is used for most prototypes in this work. Color images are available online.

requirements. To illustrate this, we compare three different combinations of fabric type and stitch design in Figure 11, which shows that combinations yield distinct patterns of stretchability in the assembled FFMS (Fig. 11, blue arrows).

If a wrinkling step is omitted, a two-way or four-way stretchable fabric must be used to accommodate the axial strains that are required for an FFMS actuator to function. A side- or cross-stitch pattern may be used with either stretchable or nonstretchable fabrics, with or without wrinkling constraints (Fig. 11, red arrows). Cross-stitching is preferred for use with four-way stretch fabrics, because it minimizes undesired radial expansion (i.e., ballooning) of the elastic tubes. Significant ballooning only occurs if side-stitch patterns are used. Commercial two-way stretch fabrics (which are typically knit) admit fabric extension in all directions, and would yield undesirable ballooning unless a cross-stitch is used. This can result in failure (Fig. 7C).

When nonstretchable fabric is used, wrinkling must be applied. In such cases, the range of extension is determined by the extent of wrinkling. In practice, we have designed FFMS actuators capable of >300% strain using this technique. If a cross-stitch is used, the amount of wrinkling is limited due to the increased fabric constraint imposed by the cross-stitch, thus limiting extensibility.

Among thread types, inextensible high-strength nylon thread can provide a stiff constraint via a fine thread. There are several possible combinations of stitch designs, fabric stretchability, and wrinkling modes, which together yield distinct patterns of stretchability in the assembled FFMS (Fig. 11, blue arrows; longer arrows imply larger stretchability). When side-stitches are used, zig-zag stitching is recommended for use with stretchable fabrics to preserve the fabric elasticity. Straight stitching is appropriate for nonstretchable fabrics, where stretching is accommodated by wrinkling. To maximize stretchability in the axial direction and minimize radial expansion, two-way stretch fabric with side-stitches and wrinkling is optimal, although nonstretch fabric with side-stitches and wrinkling is also effective. Figure 4A shows four prototypes with different combinations of fabrics and stitchings.

Tube and fluid selection

The elastic tube may be any elastomer that is compatible with the working fluid. For high-force applications, tubing materials with high elastic modulus and high extensibility would be preferred. The tube can have any diameter and length compatible with the fabrication process, including very fine silicone tubing[62] or larger diameter latex rubber tubing. There are many options among commercially available tubes (Fig. 4B). We present a model of the actuator performance accounting for effects of tube size and material properties in the Analytical Modeling section, and experimental results for several examples in the Results section.

Different working fluids may be used, depending on the performance requirements, materials, and operating criteria. In hydraulic operation, FFMS can use incompressible fluids such as oils or waters, as illustrated in many of our experiments. This makes it possible to control the applied volume in the actuator and hence the actuator length, due to the circumferential constraints, and renders the quasistatic response of the actuator very simple, at the expense of increased viscosity and mass. (However, the fluid mass in many of our

prototypes is on the order of a few grams). Low-viscosity liquids offer improved actuation speed and efficiency. Pressures in prototypes described here are lower (<0.75 MPa) than those used in industrial hydraulics (e.g., 20 MPa). At such low working pressures, failures typically involve, at most, fluid leakage.

In pneumatic operation, compressible fluids such as air or other gases may be used. This can minimize mass and viscosity. Over the operating range tested in our experiments, pneumatic operation leads to increased hysteresis, lower efficiency, and increased response latency (Fig. 6F). Further discussions of hydraulic and pneumatic actuation methods are provided in the literature.[63,64]

Analytical Modeling

As our experiments demonstrate, FFMS actuators may be operated to yield a variety of motion or force patterns. The simplest involve the generation of axial forces through a parallel configuration of N elastic tubes. Such a structure is similar to parallel muscle sheet architectures in biology. A net external force, F_{ext}, is produced by the actuator due to the stretching of the tubes, producing a net elastic force, F_{el}. The fabric can also contribute an elastic force, F_{fab}. The force F_{ext} exerted by the actuator decreases with increasing fluid pressure, p, due to the axial force, F_{fluid}, generated via the fluid pressure. Dissipative forces, F_d, include viscosity and friction. Combining these factors, one can model force production as follows:

$$F_{ext} = F_{el} + F_{fab} - F_{fluid} + F_d \qquad (1)$$

The dissipative forces, F_d, include hydrodynamic flow resistance, $F_{d,hyd}$, and dry friction at the tube fabric interface, $F_{d,dry}$:

$$F_d = F_{d,hyd} + F_{d,dry} \qquad (2)$$

$F_{d,hyd}$ can be estimated from Newton's law of viscosity[65]:

$$F_{d,hyd} = \tau \mathcal{A} = \mu \rho \frac{\partial u}{\partial y} 2\pi r_i L \qquad (3)$$

where τ is the shear stress of the fluid acting on the inner wall of the tube, $\mathcal{A}$ is the contact area between the fluid and tube, μ is the kinematic viscosity, ρ is the fluid density, u is the flow velocity, $\partial u/\partial y$ is the rate of shear deformation, r_i is the tube inner radius, and L is the tube length. The dry friction $F_{d,dry}$ is given by the following:

$$F_{d,dry} = \mathcal{F}_\mathcal{N} \zeta = N\zeta p A_{tf}, \quad A_{tf} = 2\pi r_o L \qquad (4)$$

where N is the number of tubes, ζ is the friction coefficient, $\mathcal{F}_\mathcal{N}$ is the normal force between tube and fabric, $A_{tf} = 2\pi r_o L$ is the area of the tube/fabric interface, r_o is the tube outer radius, and p is the fluid pressure. We refer to such dissipative forces when interpreting measurements of actuator efficiency and hysteresis.

In many embodiments, including the wrinkling construction described above, there is little relative motion of tube and fabric, so $F_{d,dry}$ may be neglected. In quasihydrostatic

operation, the forces due to flow resistance $F_{d,hyd}$ may also be neglected. For fabric that is wrinkled or stretchable, the fabric force, F_{fab} may also be neglected.* Assuming that these conditions hold and that the FFMS operate in a linear elastic regimen with elastic modulus E and true strain $\varepsilon = \log{(L - L_0)}$, the net external force exerted by the actuator is as follows:

$$F_{ext} = F_{el} - F_{fluid}, \tag{5}$$

where

$$F_{el} = NE\varepsilon A_{tube} = NE\varepsilon\pi(r_o^2 - r_i^2) \tag{6}$$

$$F_{fluid} = NpA_{fluid} = Np\pi r_i^2 \tag{7}$$

The result may be written as follows:

$$F_{ext} = N(E\varepsilon A_{tube} - pA_{fluid}) \tag{8}$$

The external force F_{ext}, reaches its maximum value if the fluid pressure $p = 0$:

$$\max_p F_{ext} = F_{ext}\big|_{p=0} = NE\varepsilon A_{tube}. \tag{9}$$

The force can be maximized by increasing the net cross-section area, NA_{tube}, the elastic modulus, E, or the operating range of strains, ε. Increasing the strain may be accomplished via pretensioning, which is also aided by wrinkling. The model given by Equation (8) predicts that F_{ext} decreases linearly with the increase in pressure, p. As our experiments demonstrate, despite the simplifications involved in this model, it provides a good approximation to the behavior of FFMS actuators (Sec.6, Fig. 5D4 and G4).

The minimum external force magnitude occurs when the pressure is maximum, p_{max}. Since pressure fluctuates in dynamic operation, we take this to be the maximum quasihydrostatic pressure. If the operating range of forces extends down to $F_{ext} = 0$, the required maximum pressure, p_{max}, is determined by the ratio of tube and fluid areas and tube elasticity:

$$p_{max} = \frac{E\varepsilon A_{tube}}{A_{fluid}}. \tag{10}$$

Where A_{tube} is the inner cross-section area of the tube. Conversely, if p_{max} is the maximum intended pressure, the tube geometry, strain, and elasticity should be selected to ensure this expression holds.

In another configuration, the actuator may be operated as a muscular hydrostat.[66] For unsupported (isochoric) operation, or for negative contraction forces, $F_{ext} < 0$, the muscle force may be produced by applying pressures higher than the one specified in (10). In the absence of an external load force, $F_{ext} = 0$, a pressure p applied to hydrostatic configuration can

---

*Selecting a stiffer fabric, or adding nonfluidic elastic fibers to the structure, increases forces, but does not necessarily improve actuator performance, because the added elasticity does not impart any added strength to the tube that would enable it to operate at higher pressures.

yield a displacement, δL, with respect to the initial tube length, L_0, :

$$\delta L = L_0 \exp\left(\frac{p}{E}\right) - L_0 \tag{11}$$

Such modes of operation are analogous to muscular hydrostats in biology, such as the tongues of many animals, or the elephant trunk.

FFMS actuators may also be used to compress enclosed objects. If an actuator with pressure $p > 0$ perfectly encloses a rigid cylindrical object, compressive pressures are generated as the fluid pressure p is reduced. For a cylinder of radius $r_c \ll h$, where h is the effective FFMS thickness, the thin-walled vessel equation, $\sigma_\theta = F_{ext}/A_M$, relates the compressive pressure, p_c (the force per unit area exerted on the cylinder, which may also be approximated by the internal pressure p), to the net effective cross-section area, A_M, the radius, and the thickness. Solving for p_c yields the following:

$$p_c = \frac{hF_{ext}}{r_c A_M}. \tag{12}$$

Results

To evaluate the FFMS actuators, we performed mechanical testing in several experimental configurations and operating modes, using several FFMS actuators of different sizes. We also realized functional prototypes for wearable devices, haptic feedback, and soft robotics.

Mechanical testing

We used three testing configurations to measure axial forces, compressive forces, and axial displacements. We complemented these evaluations with measurements of actuation efficiency and durability over thousands of cycles.

Mechanical testing was performed using two different prototypes (Fig. 5). The first comprised smaller surface area FFMS with three elastic tubes (Fig. 5B) of dimensions 196 mm (length), 25.2 mm (width), and 4.7 mm (thickness). The fabric channel width was 5 mm. The active area spanned by the elastic tubes was measured to be 122.4 mm in length with no applied pressure. The tubes were connected via a manifold to the fluidic power source. We used latex tubes with outer diameter 3.2 mm and inner diameter 1.6 mm.

The second prototype consisted of larger surface area FFMS with 10 parallel elastic tubes (Fig. 5C). The tubes in this prototype were connected in series, yielding a single fluid port. The dimensions of this prototype are as follows: 148.4 mm length, 156.6 mm width, 4.9 mm thickness, and 5 mm channel width. The active region spanned by the elastic tubes (neglecting unwrinkled end sections) was 84.1 mm.

In all experiments, distilled water was used as a working fluid. In a separate experiment, we compared the operating efficiency of water (hydraulic mode) and air (pneumatic mode).

Axial force testing. Axial force testing was performed using an isometric test configuration and apparatus (Fig. 5A). One end of the FFMS was fixed using a clamp fixture, while the other end was attached to a stationary force gauge (M5-

20, Mark 10). Fluid was supplied via three 10-mL syringes (inner diameter around 15 mm) driven by a displacement-controlled linear motor (A-BAR300BLC-E01; Zaber) and custom fixture. The syringe displacement was measured via an optical encoder (S6S-1000-IB; US Digital). Fluid pressure was measured using a fluid sensor (SSC Series Sensor; Honeywell) positioned near the actuator port. The actuator was prepressurized to ~650 kPa and fixed in an isometric configuration with sufficient tension to ensure that the actuator remained stationary.

The FFMS were driven via sinusoidal fluid displacement, at frequencies from 0.2 to 0.4 Hz. This yielded time-varying (measured) pressures ranging from 200 to 750 kPa. The signals were recorded synchronously using a computer-in-the-loop system (QPIDe; Quanser, Inc., with Simulink, The MathWorks, Inc.). The instantaneous displacement of fluid volume was calculated from the syringe displacement and geometry.

The FFMS performance was consistent over repeated cycles. The generated axial force decreased monotonically with the increase of fluid pressure or volume (Fig. 5D–G). The range of forces F_{ext} (Fig. 5D2–D4) generated by the FFMS was 13 N (~4.3 N per tube). This corresponded to a fluid volume range of 1.78 mL. The volume/force and the volume/pressure curves both exhibit hysteresis, indicating that energy was lost on each working cycle. We discuss such losses in the efficiency measurements below.

We compared the results with predictions of the analytical model [Eq. (8)]. To compute these predictions, we measured the Young's modulus of the elastic tube. Using tensile testing, we determined the Young's modulus to be 1.1 MPa for true strains, ε, between 0 and 1. Other parameters used for model prediction were $A_{tube} = 5.9 \times 10^{-6}$ m^2, $\varepsilon = 0.8$, and $A_{fluid} = 7.7 \times 10^{-6}$ m^2. The number of tubes was $N = 3$ for the first and $N = 10$ for the second. The experimental results and model predictions were in close agreement during slow actuation (Fig. 5D4). For different frequencies, ranging from 0.2 to 5.0 Hz, the FFMS actuator responded in a qualitatively similar manner (Fig. 5E, F). The response became somewhat more complex at the highest frequencies. This can be explained by the inherent dynamics of fluid-elastomer-fabric systems.

We obtained results when testing the larger FFMS actuator with 10 parallel tubes (Fig. 5G1–G4). In this case, the FFMS produced forces ranging from 0 to 50 N with respect to the decrease of fluid volume (from 0 to 6 mL) or fluid pressure (from 620 to 180 kPa). The FFMS performance was also consistent over repeated testing cycles. Each of the 10 tubes produced about 5 N. For the smaller prototype, analytical modeling yielded qualitatively good agreement with the experimental results (Fig. 5G4).

The results revealed a slightly nonlinear and hysteretic relationship between pressure and force, with modest discrepancies from the linear model predictions. The hysteresis can be attributed to the fact that the tubes were connected in series, requiring the fluid to traverse a much longer path. This also indicates that series connections of elastic tubes, which simplify assembly, may introduce modest response latency. From the experimental data, we estimated the latency to be ~100 ms at 0.2 Hz. The volume/pressure and volume/force relationships also exhibited hysteresis, indicating that energy was lost on each cycle. For small changes in fluid volume, from 0 to 2 mL, the change in force with fluid pressure was

more gradual. However, the pressure/force relationship remained approximately linear.

Compression testing. We evaluated the compression force, $F_c = p_c A$, produced using an FFMS prototype with three channels (Fig. 5H), where p_c was the compressive pressure. The actuator was wrapped around a cylinder in an isometric test fixture using a force sensor (ATI Nano17; ATI Industrial Automation). The contact area, A, was 209 mm^2. We varied the applied fluid volume from 0 to 2 mL (Fig. 5I). This yielded compressive forces ranging from 0 to 10 N.

These values were consistent with our predictions based on the range of axial forces, F_{ext}, produced by the same device: at fluid pressure $p = 250$ kPa, we measured the axial force to be $F_{ext} = 13$ N. The model predicts a compressive pressure $p_c = 44.5$ kPa for our text fixture configuration, which implies $F_c = p_c A = 9.3$ N, in close agreement (error <5%) with our measurements (Fig. 5K). The results varied little for speeds below 5.0 Hz.

Displacement. We performed displacement testing using a configuration that was similar to the one we used in axial force testing (Fig. 6A). For testing, a constant force retractor (Force 4.45N, model 61115A2; McMaster-Carr) was used to replace one of the isometric constraints in the fixture described above. An optical encoder was used to record the position for the distal end of FFMS. Displacement increased with increases of fluid volume or fluid pressure. The results revealed consistent displacement across repeated actuation (Fig. 6B1). As predicted, the relationship between volume and displacement was almost perfectly linear, reflecting the incompressibility of the medium and radial constraint provided by the textile (Fig. 6B2). When the fluid volume reached 4.5 mL, the FFMS attained a length increase of 70% (from 122.4 to 207.4 mm).

In this case, the volume/pressure and pressure/displacement relationships exhibited greater hysteresis. We attributed this to the deformation of the nonlinear elastic materials at large displacements or high fluid volumes (Fig. 6B3, B4). The analytical model correctly predicted the observed ranges of displacement, but because the model was quasistatic, it did not capture hysteresis. We plan to develop a dynamic model that can capture such effects in future work. We also observed that the performance of FFMS remained consistent at higher driving frequencies. The results for the larger FFMS with 10 channels were similar to those that we observed for the smaller FFMS (Fig. 6E1–E4).

Efficiency. We computed the energetic efficiency as the ratio of the input energy and the mechanical work over one working cycle. We measured this for a single-channel FFMS with different working fluids, comprising water (hydraulic mode) and air (pneumatic mode).

The FFMS (rest channel length and width 62 and 10 mm, tube outer and inner diameters 6.4 and 3.2 mm) raised a load of mass m against gravity at speed of $v = 0.1$ mm/s to height h. Input work, W_{in}, was computed as the sum of (positive) mechanical work, W_+, performed when extending the actuator, and (negative) work, W_-, performed when withdrawing the fluid (during lifting), yielding $W_{in} = W_+ + W_-$. The energy efficiency, R, was $R = U_g / W_{in}$, where $U_g = mgh$ was the output work, or change in potential energy of the mass

over one working cycle. The results were averaged over five working cycles in which the actuator returned to its initial state after displacing the mass.

The actuator efficiency was higher in hydraulic operation than in pneumatic operation (efficiency $R = 0.46$ vs. 0.25) (Fig. 6F). This can be explained by the additional thermodynamic losses arising from the compression of air. Other losses included those due to fluid viscosity, friction, and thermoelastic heating of the elastomer.

Prior authors[26] computed the efficiency of a soft fluidic actuator by considering the work W_- performed when withdrawing the fluid as an output of the system, yielding $R = (U_g + W_-)/W_+$. However, such a calculation leads to erroneous results, since a system can be designed to make the efficiency arbitrarily close to 1 by adding and removing an increment of fluidic energy at the input without any additional production of useful work (e.g., this can be achieved by adding a reservoir at the input). Applying this method to our actuator, we obtained a (erroneous) higher efficiency of $R = 0.83$ in hydraulic operation.

We also evaluated the efficiency of a hydraulically driven three-channel FFMS (rest channel length and width 44 and 5 mm, latex tube outer and inner diameters 3.2 and 1.6 mm). The results were thus similar to those that we obtained with the single-channel device ($R = 0.45$, based on five repeated measurements).

Durability. We evaluated the durability of FFMS (three-channel prototype) (Fig. 6G) by actuating it over 5000 cycles to a maximum amplitude of 28 mm. The behavior was similar throughout testing. A 5% reduction in displacement was observed after this testing cycle. We attributed this to initial relaxation of elastic tube and fabric material. The relatively consistent performance may be attributed, in part, to the operation of the tube within the elastic regimen, which resulted in little plastic yielding.

Failure modes. Actuator failure can arise due to improper selection of material, assembly, or operation regimen. Here, we highlight three failure modes observed in our prototypes during the experiments (Fig. 7). As the fluid pressure increases, the elastic tubes, enclosed fabrics, and stitches are subjected to the increase of stresses. This can result in fabric tearing, stitch failure, or ballooning of the elastic tube. Fabric tearing can be minimized through the use of high-strength or dense fabrics, ideally with thread counts exceeding 300.

One failure mode was associated with a large cross-section elastic tube. For fixed fluid pressure, p, the force per unit length, t_s, exerted on the stitch is proportional to pr_o, where r_o is the tube outer radius. As the tube radius is increased, stitch failure will occur when t_s exceeds a critical value. Such stitch failures may be minimized through the use of high-strength threads, composed of materials such as polyester or poly-paraphenylene terephthalamide (Kevlar), through multiple (double or triple) stitching, and through the use of stronger fabrics.

Another failure mode arose from insufficient radial constraints on the elastic tube, which yielded radial expansion or ballooning of the tube. We observed this to occur due to imperfections in side stitching, due to gaps between cross-stitches, or due to the use of four-way stretchable fabrics. Such failures may be mitigated via uniform stitching, by avoiding four-way stretch fabric, and, where two-way stretch fabrics are used, via zig-zag stitching with fine pitch.

FFMS Embodiments and Applications

FFMS actuators are versatile and capable of actuating a variety of bodies or structures of different scales. They can be designed to realize multiple modes of actuation that are suited to applications in robotics, health care, and wearable technologies, as illustrated below.

Scalability

FFMS actuators can be used to realize devices of different sizes, ranging from millimeter- to meter-scale devices. The dimensional parameters of the FFMS include the lengths, L, of the elastic tubes, their inner and outer radii, r_i and r_o, and number, N, of elastic tubes. These parameters determine the stitched conduit width, fabric length, and fabric width. For fixed material, tube configuration, and strain, the maximum force is determined by $r_o^2 - r_i^2$. The maximum elongation, ΔL, is proportioned to L. The required maximum pressure is scale invariant [Eq. (10)]. Commercially available elastic tubes can be used with widely varying radii, r_i, r_o, ranging from <1 to >30 mm.

We fabricated several prototypes to explore the scaling of FFMS actuators (Fig. 8) for different applications (Fig. 10). Small, low-profile FFMS may be used in miniature biomedical or wearable devices, while large FFMS can be used in higher force applications, such as orthotics or soft robotic construction machines.

Multimodal actuation and shape change

Composite or multiactuated FFMS can yield dynamic, multimodal motion or shape change. Here, we show how FFMS actuators can be used to realize in-plane rotation, out-of-plane bending, and biaxial bending motion (Fig. 9).

In-plane rotation may be realized by differentially driving multiple fluid channels to steer an actuator. Such motions may be used in soft biomedical devices.[67] In one embodiment, 3 cm FFMS are driven via three elastic tubes that are independently controlled. When one of three lateral tubes is depressurized, a large-amplitude planar rotation can be achieved, yielding turning angles approaching 90° (Fig. 9A) due to differential elongation in the three tubes.

Out-of-plane bending motion can also be achieved. We combined a passive layer of stiff fiberglass with FFMS to produce continuous out-of-plane bending. In one embodiment, a fiberglass sheet (thickness 0.38 mm) was pre-patterned via laser engraving and stitched to the FFMS (Fig. 9B). Pressurizing the FFMS yielded large-amplitude bending, exceeding 180°. Selecting the bending stiffness of the passive layer makes it possible to tune the actuator stiffness and generated torques. Such a configuration may be used in wearable or soft robotic applications.[68]

If two FFMS layers are oriented in complementary directions, biaxial bending or three-dimensional (3D) shape change, may be generated. To demonstrate this capability, we stitched two seven-channel FFMS layers together in orthogonal orientations (Fig. 9C). The whole composite structure remained flat when the applied fluid pressure was equal in both FFMS layers. When the applied fluid pressures were

unequal in each layer, bending motion was initiated about in each of the two orthogonal in-plane axes. Biaxial bending yielded 3D or hyperboloid shapes.

Device configurations and applications

FFMS may be used to realize motion or provide forces in applications, including soft robotic motion control, wearable actuators, assistive devices, and compression garments. Some advantages of these devices include their low cost, flexible design, facile fabrication, ability to conform to curved structures, to achieve multimodal actuation at a variety of scales, to produce large work densities, and achieve fast response times, exceeding the capabilities of many other technologies.

We realized several examples (Fig. 10 and Supplementary Videos S1 and S2). Miniature FFMS can be used to produce linear motion, to provide skin stretch haptic feedback, or to provide compression forces to small body parts, such as a finger (Fig. 10D, E). We also fabricated three-channel FFMS that can contract from 10.5 mm in to 5 mm in length, lifting a mass of 500 g, while producing engineering strains up to 110% (Fig. 10A). Other compact devices can be used to apply constriction to small body parts (Fig. 10D, showing FFMS of 1 mm thickness). They can also be used to realize wearable devices for providing haptic feedback via skin-stretch, yielding highly palpable tactile sensations (Fig. 10E).

Larger scale FFMS actuators can perform greater mechanical work. We fabricated a 10-channel device that can lift a 3 kg mass (Fig. 5C). This was 115 times higher than the actuator mass of 26 g (Fig. 10B, left). We realized a larger FFMS actuator with three tubes (inner latex tube of diameter 25 mm, outer diameter of 32 mm), which lifted a 15 kg mass at fluid pressures <276 kPa (Fig. 10B, right). This demonstrates how FFMS actuators can be used to perform significant mechanical work.

FFMS actuators hold promise for wearable applications such as assistive devices. We used a configuration similar to the one we used for out-of-plane bending (Fig. 9C) to provide assistive flexion forces for two fingers during grasping (Fig. 10C). In this application, we pretensioned the fiberglass sheet layers such that the device performed flexion when pressurized and extension when depressurized (Fig. 10C, bottom inset). The force was sufficient to open and close the hand for grasping. Such a device is useful for assisting conditions such as stroke that can often lead to chronic flexion of the fingers, preventing grasping and adversely affecting many activities of daily living.[8,68]

FFMS devices can also be used to provide compression to larger areas of the extremities. Such compressive forces are of interest for haptic feedback,[69] for preventative compression therapy in deep vein thrombosis,[70] for musculoskeletal recovery via blood flow restriction therapy,[71,72] for lymphatic or cardiovascular circulatory conditions,[73,74] or other biomedical devices.[75–78]

We created an upper limb compression device based on an FFMS arm band and measured the resulting compressive pressures using thin-film force sensors (FlexiForce A201; Tekscan, Inc.). Withdrawing up to 3 mL of fluid from the band yielded uniform compression of up to 12 kPa, similar to pressures provided by blood pressure cuffs.

We also demonstrate a wearable compression garment for the lower limb (Fig. 10G). This device is constructed from three elastic tubes arranged in three independently controlled sections (Fig. 10G, dashed boxes). Supplying different fluid pressures to different sections yields varied compressive pressures across the limb. This can be used to provide bulk compression to the limb, which is useful in recovery from some injuries or in disease treatment. It can also be used for providing dynamic peristaltic motions that can be used for undulatory massage to augment lymph and blood flow. Such devices can meet the needs for pressure garment therapy,[76] lymphedema treatments,[77] or venous closure treatments.[78]

Conclusions

This article presents a new family of soft actuators that we refer to as FFMS, inspired by sheet-like biological muscles. These devices comprise fabric layers with integrated hydraulic transmissions formed from arrays of hollow elastic tubes routed in patterned fabric conduits. We demonstrate how to design and fabricate these devices using facile methods that build on apparel engineering techniques, including computerized sewing processes. These devices are stretchable, conformable, safe, efficient, and scalable. They are applicable to small, millimeter-scale actuators, and large meter-scale devices, and can yield forces exceeding 150 N, more than 115 times their weight, with engineering strains >100%. Laboratory prototypes perform consistently in testing over thousands of cycles. Their performance can be predicted via simple mechanical modeling, aiding design.

As we show, such FFMS actuators hold promise for applications in soft robotic motion control and for wearable devices for haptics, health care, and assistive technologies. The compressions they can produce meet requirements for several health care applications.

These results also point to several promising areas for future investigation. The fabrication methods we describe are simple and flexible, but further research is needed to align them with manufacturing techniques. FFMS actuators prove capable of performance in axial actuation, compression, and multimodal actuation, where dynamic shapes or stresses are enabled by designed routings of fluidic channels. New analytical and computational design methods would facilitate a larger variety of programmable distributions of forces and strains, and would enable greater control over such behaviors. The performance of FFMS actuators depends on the fluidic power source that is used. We highlighted advantages of hydraulic operation. Further research is needed on compact hydraulic power sources.

The analytical model we present was effective for predicting actuator performance, but the model is quasistatic. In future work, we plan to extend this approach to account for dynamics, aiding precise real-time control. Our devices use open-loop control strategies, and the performance of these devices would be further improved through the use of closed-loop controllers relying on fluidic or strain sensors. Intrinsic mechanical or physiological sensors would enable further applications.

The demonstration cases we present highlight potential applications in wearable devices for human/computer interaction and virtual reality. We anticipate investigating these in future work. Our demonstrations also point to a range of potential biomedical applications for assistive and therapeutic devices. These merit further research. We have highlighted applications of FFMS actuators in several forms of wearable devices. Our design and fabrication methods are

amenable to realizing integrated garments that may be applied to larger body areas, including the realization of whole-body actuated suits or soft exoskeletons, which could greatly aid applications in haptic virtual reality, human space exploration, and rehabilitation. We intend to explore such garments and applications in future work.

Symbols Used

Symbol = description
F_{fluid} = axial force produced via fluid pressure
F_{ext} = axial external load force
F_{el} = axial elastic force of tubing
F_{fab} = axial force due to fabric
F_d = dissipative forces including viscosity and friction
$F_{d, hyd}$ = hydrodynamic flow resistance force
$F_{d, dry}$ = dry friction force at tube/fabric interface
τ = shear stress of fluid at inner wall of tube
$\mathcal{A}$ = contact area between fluid and tube
μ = kinematic viscosity of fluid
ρ = fluid density
$\frac{\partial u}{\partial y}$ = rate of shear deformation of fluid
r_i = tube inner radius
L = tube length
$\mathcal{F}_{\mathcal{N}}$ = normal force between tube and fabric
ζ = friction coefficient
p = fluid pressure
r_o = tube outer radius
N = number of elastic tubes
E = tube elastic modulus
ε = tube true strain
A_{tf} = area of the tube/fabric interface
A_{tube} = cross-section area of a single tube
A_{fluid} = cross-section area of fluid inside a single tube
δL = tube displacement
L_0 = initial tube length
h = effective FFMS thickness
r_c = radius of a cylindrical object
A_M = effective axial cross-section area of FFMS

Acknowledgment

Author Disclosure Statement

No competing financial interests exist.

Funding Information

Supplementary Material

Supplementary Video S1
Supplementary Video S2

References

1. Yap HK, Ng HY, Yeow C-H. High-force soft printable pneumatics for soft robotic applications. Soft Robot 2016; 3:144–158.

2. Booth JW, Shah D, Case JC, *et al*. OmniSkins: Robotic skins that turn inanimate objects into multifunctional robots. Sci Robot 2018;3:eaat1853.

3. Rus D, Tolley MT. Design, fabrication and control of soft robots. Nature 2015;521:467.

4. Song YS, Sun Y, Van Den Brand R, *et al*. Soft robot for gait rehabilitation of spinalized rodents. In 2013 IEEE/RSJ International Conference on Intelligent Robots and Systems, Tokyo, Japan, IEEE, 2013, pp. 971–976.

5. Park Y-L, Chen B-R, Pérez-Arancibia NO, *et al*. Design and control of a bio-inspired soft wearable robotic device for ankle–foot rehabilitation. Bioinspir Biomim 2014;9:016007.

6. Park Y-L, Chen B-R, Majidi C, *et al*. Active modular elastomer sleeve for soft wearable assistance robots. In 2012 IEEE/RSJ International Conference on Intelligent Robots and Systems, Vilamoura, Portugal, IEEE, 2012, pp. 1595–1602.

7. Koo IM, Jung K, Koo JC, *et al*. Development of soft-actuator-based wearable tactile display. IEEE Trans Robot 2008;24:549–558.

8. Polygerinos P, Wang Z, Galloway KC, *et al*. Soft robotic glove for combined assistance and at-home rehabilitation. Robot Auton Syst 2015;73:135–143.

9. Cotin S, Delingette H, Ayache N. Real-time elastic deformations of soft tissues for surgery simulation. IEEE Trans Visual Comput Graphics 1999;5:62–73.

10. Serchi FG, Arienti A, Laschi C. Biomimetic vortex propulsion: Toward the new paradigm of soft unmanned underwater vehicles. IEEE/ASME Trans Mech 2013;18:484–493.

11. Kwon GH, Park JY, Kim JY, *et al*. Biomimetic soft multifunctional miniature aquabots. Small 2008;4:2148–2153.

12. Wang W, Rodrigue H, Ahn S-H. Deployable soft composite structures. Sci Rep 2016;6:20869.

13. Kim S, Laschi C, Trimmer B. Soft robotics: A bioinspired evolution in robotics. Trends Biotechnol 2013;31:287–294.

14. Cutter C. A Treatise on Anatomy, Physiology, and Hygiene. London, UK: JB Lippincott & Company, 1852.

15. Marchese AD, Katzschmann RK, Rus D. A recipe for soft fluidic elastomer robots. Soft Robot 2015;2:7–25.

16. Daerden F, Lefeber D. Pneumatic artificial muscles: Actuators for robotics and automation. Eur J Mech Environ Eng 2002;47:11–21.

17. Schulte H, Jr. The Characteristics of the McKibben Artificial Muscle. The Application of External Power in Prosthetics and Orthotics. Washington DC: National Academy of Sciences-National Research Council, Appendix H, 1961, pp. 94–115.

18. Gavrilović M, Marić M. Positional servo-mechanism activated by artificial muscles. Med Biol Eng 1969;7:77–82.

19. Chou C-P, Hannaford B. Measurement and modeling of McKibben pneumatic artificial muscles. IEEE Trans Robot Autom 1996;12:90–102.

20. Tondu B, Lopez P. Modeling and control of McKibben artificial muscle robot actuators. IEEE Control Syst 2000; 20:15–38.

21. Tondu B, Lopez P. Theory of an artificial pneumatic muscle and application to the modeling of McKibben artificial muscle. Comptes rendus de l'Académie des sciences. Série II, Mécanique, physique, chimie, astronomie 1995;320:105–114.

22. Hunter IW, Hollerbach JM, Ballantyne J. A comparative analysis of actuator technologies for robotics. Robot Rev 1991;2:299–342.

23. Bishop-Moser J, Krishnan G, Kim C, *et al*. Design of soft robotic actuators using fluid-filled fiber-reinforced elastomeric

enclosures in parallel combinations. In 2012 IEEE/RSJ International Conference on Intelligent Robots and Systems, Vilamoura, Portugal, IEEE, 2012, pp. 4264–4269.

24. Connolly F, Polygerinos P, Walsh CJ, *et al*. Mechanical programming of soft actuators by varying fiber angle. Soft Robot 2015;2:26–32.

25. Hawkes EW, Christensen DL, Okamura AM. Design and implementation of a 300% strain soft artificial muscle. In 2016 IEEE International Conference on Robotics and Automation (ICRA), Stockholm, Sweden, IEEE, 2016, pp. 4022–4029.

26. Sridar S, Majeika CJ, Schaffer P, *et al*. Hydro Muscle-a novel soft fluidic actuator. In 2016 IEEE International Conference on Robotics and Automation (ICRA), Stockholm, Sweden, IEEE, 2016, pp. 4014–4021.

27. Cappello L, Galloway KC, Sanan S, *et al*. Exploiting textile mechanical anisotropy for fabric-based pneumatic actuators. Soft Robot 2018;5:662–674.

28. Martinez RV, Fish CR, Chen X, *et al*. Elastomeric origami: Programmable paper-elastomer composites as pneumatic actuators. Adv Funct Mater 2012;22:1376–1384.

29. Li S, Vogt DM, Rus D, *et al*. Fluid-driven origami-inspired artificial muscles. Proc Natl Acad Sci U S A 2017;114: 13132–13137.

30. Yang D, Verma MS, So J-H, *et al*. Buckling pneumatic linear actuators inspired by muscle. Adv Mater Technol 2016;1:1600055.

31. Otsuka K, Wayman CM. Shape Memory Materials. Cambridge, UK: Cambridge University Press, 1999.

32. Kim S, Hawkes E, Cho K, *et al*. Micro artificial muscle fiber using NiTi spring for soft robotics. In IROS 2009, IEEE/RSJ International Conference on Intelligent Robots and Systems, St. Louis, MO, IEEE, 2009, pp. 2228–2234.

33. Haines CS, Lima MD, Li N, *et al.* Artificial muscles from fishing line and sewing thread. Science 2014;343:868–872.

34. Li F, Chen Y, Zhu W, *et al*. Shape memory effect of polyethylene/nylon 6 graft copolymers. Polymer 1998;39: 6929–6934.

35. Takashima K, Rossiter J, Mukai T. McKibben artificial muscle using shape-memory polymer. Sens Actuators A Phys 2010;164:116–124.

36. Liu C, Qin H, Mather P. Review of progress in shape-memory polymers. J Mater Chem 2007;17:1543–1558.

37. Zhang C-S, Ni Q-Q. Bending behavior of shape memory polymer based laminates. Compos Struct 2007;78:153–161.

38. Jung K, Nam J, Choi H. Investigations on actuation characteristics of IPMC artificial muscle actuator. Sens Actuators A Phys 2003;107:183–192.

39. Guo S, Ge Y, Li L, *et al*. Underwater swimming micro robot using IPMC actuator. In Proceedings of the 2006 IEEE International Conference on Mechatronics and Automation, Luoyang, China, IEEE, 2006, pp. 249–254.

40. Bhat N, Kim W-J. Precision force and position control of an ionic polymer metal composite. Proc Inst Mech Eng Part I J Syst Control Eng 2004;218:421–432.

41. Carpi F, De Rossi D, Kornbluh R, *et al*. Dielectric Elastomers as Electromechanical Transducers: Fundamentals, Materials, Devices, Models and Applications of an Emerging Electroactive Polymer Technology. Amsterdam, Netherlands: Elsevier, 2011.

42. Kellaris N, Venkata VG, Smith GM, *et al*. Peano-HASEL actuators: Muscle-mimetic, electrohydraulic transducers that linearly contract on activation. Sci Robot 2018;3:eaar3276.

43. Guo R, Sheng L, Gong H, *et al*. Liquid metal spiral coil enabled soft electromagnetic actuator. Sci China Technol Sci 2018;61:516–521.

44. Do TN, Phan H, Nguyen T-Q, *et al*. Miniature soft electromagnetic actuators for robotic applications. Adv Funct Mater 2018;28:1800244.

45. Pawashe C, Floyd S, Sitti M. Modeling and experimental characterization of an untethered magnetic micro-robot. Int J Robot Res 2009;28:1077–1094.

46. Do TN, Seah TET, Yu HK, *et al*. Development and testing of a magnetically actuated capsule endoscopy for obesity treatment. PLoS One 2016;11:e0148035.

47. Hofmann UA, Bützer T, Lambercy O, *et al*. Design and evaluation of a bowden-cable-based remote actuation system for wearable robotics. IEEE Robot Autom Lett 2018;3: 2101–2108.

48. In H, Kang BB, Sin M, *et al*. Exo-Glove: A wearable robot for the hand with a soft tendon routing system. IEEE Robot Autom Mag 2015;22:97–105.

49. Wei W, Qu Z, Wang W, *et al*. Design on the bowden cable-driven upper limb soft exoskeleton. Appl Bionics Biomech 2018;2018:1–9.

50. Yuen MC, Bilodeau RA, Kramer RK. Active variable stiffness fibers for multifunctional robotic fabrics. IEEE Robot Autom Lett 2016;1:708–715.

51. Masuda A, Ni Q-Q, Sone A, *et al*. Preliminary characterization and modeling of SMA-based textile composites. Smart Structures and Materials 2004: Modeling, Signal Processing, and Control, Vol. 5383. Bellingham, WA: International Society for Optics and Photonics, 2004, pp. 94–103.

52. Kobayashi K, Hayashi S. Woven fabric made of shape memory polymer. July 7 1992, US Patent 5,128,197.

53. Buckner TL, Kramer-Bottiglio R. Functional fibers for robotic fabrics. Multifunct Mater 2018;1:012001.

54. Niino T, Egawa S, Kimura H, *et al*. Electrostatic artificial muscle: Compact, high-power linear actuators with multiple-layer structures. In Proceedings, IEEE Workshop on Micro Electro Mechanical Systems, MEMS'94, Diso, Japan, IEEE, 1994, pp. 130–135.

55. Zhao H, Hussain AM, Duduta M, *et al*. Compact dielectric elastomer linear actuators. Adv Funct Mater 2018;28: 1804328.

56. Duduta M, Hajiesmaili E, Zhao H, *et al*. Realizing the potential of dielectric elastomer artificial muscles. Proc Natl Acad Sci U S A 2019;116:2476–2481.

57. Niiyama R, Sun X, Sung C, *et al*. Pouch motors: Printable soft actuators integrated with computational design. Soft Robot 2015;2:59–70.

58. Funabora Y. Flexible fabric actuator realizing 3D movements like human body surface for wearable devices. In 2018 IEEE/RSJ International Conference on Intelligent Robots and Systems (IROS), Madrid, Spain, IEEE, 2018, pp. 6992–6997.

59. Watanabe M, Tsukagoshi H. Suitable configurations for pneumatic soft sheet actuator to generate traveling waves. Adv Robot 2018;32:363–374.

60. Shah DS, Yuen MC-S, Tilton LG, *et al*. Morphing robots using robotic skins that sculpt clay. IEEE Robot Autom Lett 2019;4:2204–2211.

61. Drake R, Vogl AW, Mitchell AW. Gray's Anatomy for Students E-Book. London, UK: Elsevier Health Sciences, 2014.

62. Do TN, Visell Y. Stretchable, twisted conductive micro-tubules for wearable computing, robotics, electronics, and healthcare. Sci Rep 2017;7:1753.

63. De Volder M, Reynaerts D. Pneumatic and hydraulic microactuators: A review. J Micromech Microeng 2010;20:043001.

64. Polygerinos P, Correll N, Morin SA, et al. Soft robotics: Review of fluid-driven intrinsically soft devices; manufacturing, sensing, control, and applications in human–robot interaction. Adv Eng Mater 2017;19:1700016.

65. Batchelor CK, Batchelor G. An Introduction to Fluid Dynamics. Cambridge, UK: Cambridge University Press, 1967.

66. Kier WM, Smith KK. Tongues, tentacles and trunks: The biomechanics of movement in muscular-hydrostats. Zool J Linnean Soc 1985;83:307–324.

67. Berthet-Rayne P, Gras G, Leibrandt K, et al. The i 2 snake robotic platform for endoscopic surgery. Ann Biomed Eng 2018;46:1663–1675.

68. Noritsugu T, Yamamoto H, Sasakil D, et al. Wearable power assist device for hand grasping using pneumatic artificial rubber muscle. SICE 2004 Annu Conference 2004;1:420–425.

69. Delazio A, Nakagaki K, Klatzky RL, et al. Force jacket: Pneumatically-actuated jacket for embodied haptic experiences. In Proceedings of the 2018 CHI Conference on Human Factors in Computing Systems, Montreal, Canada, ACM, 2018, p. 320.

70. Mazzone C, Grandi FC, Sandercock P, et al. Physical methods for preventing deep vein thrombosis in stroke. Cochrane Database Syst Rev 2002;1:1–21.

71. Loenneke JP, Wilson JM, Marín PJ, et al. Low intensity blood flow restriction training: A meta-analysis. Eur J Appl Physiol 2012;112:1849–1859.

72. Lowery RP, Joy JM, Loenneke JP, et al. Practical blood flow restriction training increases muscle hypertrophy during a periodized resistance training programme. Clin Physiol Funct Imaging 2014;34:317–321.

73. King M, Deveaux A, White H, et al. Compression garments versus compression bandaging in decongestive lymphatic therapy for breast cancer-related lymphedema: A randomized controlled trial. Support Care Cancer 2012;20:1031–1036.

74. Williamson J, Mitchell J, Olesen H, et al. Reflex increase in blood pressure induced by leg compression in man. J Physiol 1994;475:351–357.

75. Payne CJ, Hevia EG, Phipps N, et al. Force control of textile-based soft wearable robots for mechanotherapy. In 2018 IEEE International Conference on Robotics and Automation (ICRA), Brisbane, Australia, IEEE, 2018, pp. 1–7.

76. Duffield R, Kalkhoven J. Effects of compression garments in strength, power and speed based exercise. In: Engel F, Sperlich B, eds. Compression Garments in Sports: Athletic Performance and Recovery. Basel, Switzerland: Springer, 2016, pp. 63–78.

77. Brennan MJ, Miller LT. Overview of treatment options and review of the current role and use of compression garments, intermittent pumps, and exercise in the management of lymphedema. Cancer 1998;83:2821–2827.

78. Partsch B, Partsch H. Calf compression pressure required to achieve venous closure from supine to standing positions. J Vasc Surg 2005;42:734–738.

Address correspondence to:
Yon Visell
Department of Mechanical Engineering
University of California, Santa Barbara
Santa Barbara, CA 93106

E-mail: yonvisell@ucsb.edu